

DNA/Protein interaction and cytotoxic activity of Imidazole terpyridine derived Cu(II)/Zn(II) metal complexes †

V. M. Manikandamathavan,^a T. Weyhermüller,^b R. P. Parameswari,^c M. Sathishkumar,^a

V. Subramanian,^a and Balachandran Unni Nair,^{*a}

5

Two imidazole terpyridine (itpy) based complexes, [Cu(itpy)(OAc)(H₂O)] NO₃·H₂O (**1**) and [Zn(itpy)(OAc)]OAc (**2**) have been synthesised and characterized. The crystal structure of complex **1** shows distorted octahedral geometry with anti-parallel stacking arrangement. The interactions of the two complexes with CTDNA have been studied using absorption titration and circular dichroism.

10 Complex **1** shows coordinate binding to DNA bases, **2** shows intercalative mode of binding with DNA.

Complex **1** cleaves the DNA via oxidative pathway in the presence of additives, due to the presence of redox active copper (II) centre. Complex **2** on the other hand, cleaves DNA hydrolytically. Interactions of the two complexes with BSA have been studied using fluorescence quenching and circular dichroism experiments. Circular dichroic analysis reveals that both the complexes strongly influence 15 the secondary structure of the protein. Fluorescence quenching experiment indicates different binding sites for complexes **1** and **2** on the protein. Further, the complexes show potential cytotoxicity towards A549 lung cancerous cell line. Both the complexes have been found to induce apoptosis.

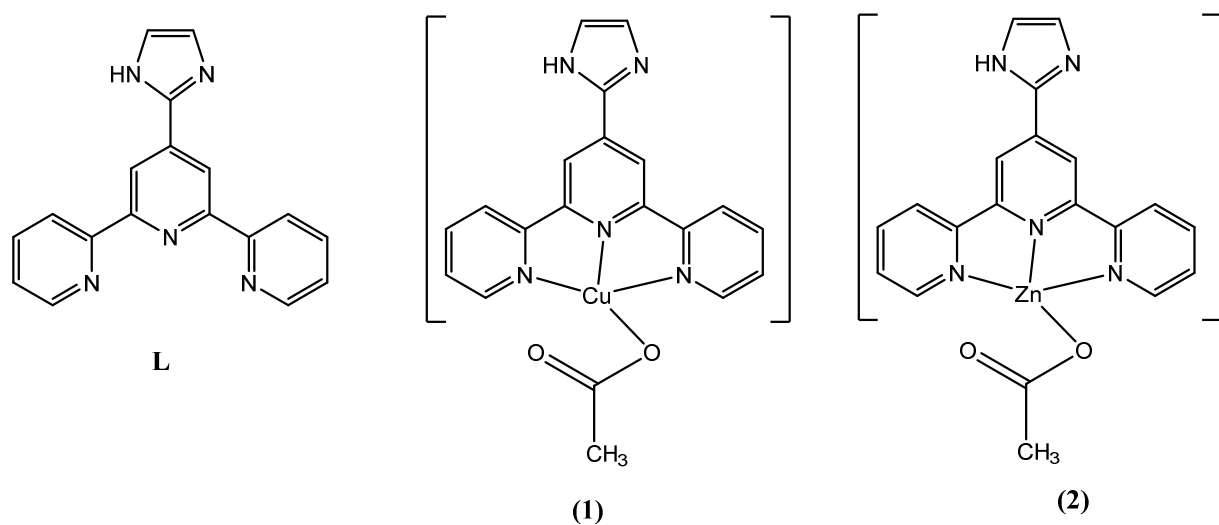
Introduction

Metal based chemotherapy for cancer has seen enough innovation, since the practice was first started using cis-platin in 1978, with the serendipitous discovery by Rosenberg et al.¹⁻³ Antitumor activity of cis-platin over trans-platin and improved second generation platinum complexes correlates the key point of structure activity relationship in the design of drug molecules.^{4, 5} Ligand structure, functionality and metal centers have undergone many changes to achieve the target selectivity. DNA and protein are the two important biological targets for anticancer drugs. Recently gene signaling pathway has also been shown to play an important role.⁶ Design of DNA and protein targeting metal based anti-cancer agents with potential *in-vitro* toxicity has gained prominence in recent time.^{7, 8} Ever since it has been found that the pioneering platinum based drugs show cellular resistance and undesirable side effects,⁹⁻¹¹ there have been efforts to develop non platinum based anticancer agents. Structural and conformation changes of DNA and protein induced by metal complexes strongly influence the biological process inside the cell. In recent years there have been efforts to investigate anticancer agents based on bio-essential metal ions such as copper (II), zinc (II) and iron (III).¹²⁻¹⁵

15 Zinc and copper are the second and third most abundant transition metal ions present in the cellular body after iron. Antagonist zinc and copper play important role in many enzymatic reactions¹⁶⁻¹⁸, which is essential for biological functions. One of the important zinc and copper enzyme, superoxide dismutase (SOD) keeps the cell safe from the metabolic wastes^{19, 20}. Imidazole, which is structurally similar to histidine residue, is a biologically important ligand for Cu (II) binding in many biological

20 systems. Metal complexes of imidazole terpyridine have recently been shown to have potential application in chemotherapy^{21, 22}. Changing the ligand environment towards the specific target is one way of tuning the selectivity of the drug molecule. Nature of the ligand is expected to play an important role in the binding of the metal complex to a biomolecule like DNA or protein. Metal complexes with ligands having extended planarity have been shown to bind to DNA intercalatively²³.

On the other hand, metal complexes with ligands lacking planar structure are known to bind to DNA non-intercalatively²⁴. The central metal ion too is expected to play a role in the efficacy of the metal complex as a drug. For example, a redox active metal ion like Cu(II) may promote transformation of the biomolecule like DNA or protein through an oxidative pathway²⁵. On the other hand, a metal ion like Zn(II), which is redox inactive is expected to behave in a different way²⁶. Hence, these two metal ions have been chosen in the present investigation. The complexes described here have unique structural features. The complexes have planar terpyridine ligand, which can serve as an intercalator; the imidazole head group has protonated as well as deprotonated nitrogen base; have different metal centres and the complexes have free labile sites which can take part in ligand exchange interaction with biomolecules. In this paper an attempt has been made to understand the effect of two different metal ions in the same ligand environment (Scheme 1), on the DNA/BSA binding ability and the cytotoxicity of the complexes.



of the species $[\text{Cu}(\text{Itpy})]^{2+}$ under the mass spectral conditions. The peak observed at m/z 421.00 can be assigned to the species $[\text{Cu}(\text{Itpy})(\text{OAc})]^+$. Formation of the species $[\text{Cu}(\text{Itpy})]^{2+}$ is a clear indication of the labile nature of the acetate ion. The ESI mass spectrum of complex **2** (Fig. S2, ESI†), shows base peak at m/z 422.27 (the Zn^{66} isotopic peak appears at 424) which can be attributed to $[\text{Zn}(\text{Itpy})(\text{OAc})]^+$ ion. The formation of complex **2** has also been confirmed from its NMR (^1H & ^{13}C) spectrum in $\text{dms}\text{-d}_6$ (Fig. S3, ESI†). Even though the acetate ligand is labile, particularly in the case of the complex **1**, as evident from the ESI-MS spectrum of this complex, the tridentate Itpy remains chelated to the metal ion. Copper(II) complexes of terpyridine ligands have been shown to be quite stable in solution with stability constant of $\text{Cu}(\text{terpy})^{2+}$ being 10^{13} M^{-1} .²⁷ UV-Visible spectrum of complex **1** and **2** in DMSO : buffer (1:50) solution is shown in Fig. S4, ESI†. Both the complexes show ligand based π - π^* transitions; at 287 nm (7000 , $\text{M}^{-1}\text{cm}^{-1}$) for complex **1** and at 285 nm (7900 $\text{M}^{-1}\text{cm}^{-1}$) for complex **2**. Charge transfer transition for copper (II) complex is observed at 337 (6850 $\text{M}^{-1}\text{cm}^{-1}$) and for the Zn(II) complex the CT band is observed at 329 nm (7500 $\text{M}^{-1}\text{cm}^{-1}$). EPR spectrum of complex **1** in DMSO at 77 K shows axial symmetry with $d_{x^2-y^2}$ as ground state (Fig. S5, ESI†). Experimental Hamiltonian parameters for **1** are g_{\parallel} (2.2500), g_{\perp} (2.0558) and A_{\parallel} (163 G). Redox behaviour of the complexes (Fig. S6, ESI†) have been investigated by cyclic voltammetry in DMSO with TBAP as a supporting electrolyte under nitrogen atmosphere using SCE as a reference, GC working and platinum wire as a counter electrode. Complex **1** shows quasi-reversible cyclic voltammogram with E_{pa} -0.134 V and E_{pc} -0.345 V which can be attributed to $\text{Cu}^{\text{II}}/\text{Cu}^{\text{I}}$ redox couple. In the case of complex **2**, irreversible cathodic peak appear at E_{pc} -0.628 V ($\text{Zn}^{\text{II}}/\text{Zn}^0$), which is less than the standard redox potential of $\text{Zn}^{\text{II}}/\text{Zn}^0$ (-0.76 eV). This may due to the chelation of the ligand.

X-ray diffraction analysis

The structure of **1** has been determined by X-ray crystallography. The crystallographic parameters are given in Table 1. The basal plane consists of one oxygen atom from acetate ion and three nitrogen atoms from planar itpy ligand. The apical sites are occupied by one water molecule and one oxygen atom from acetate ion, which is elongated due to john teller distortion. In addition to the itpy and acetate ligands, ORTEP of complex **1** (Fig. 1a) shows uncoordinated nitrate anion and two co-crystallized water molecules, which would have come from residual water in the solvent. The important bond lengths and bond angels are given in Table 2. Because of the planar nature of the itpy ligand the complexes are stacked in an antiparallel manner. Every complex molecule in the stack is connected to alternate complex molecule through hydrogen bonding between one of the O atom of the acetate ion and the coordinated water molecule as shown in Fig. 1b. The lattice water is hydrogen bonded to N atom of the imidazole moiety present in itpy ligand.

Computation methods

Optimized structure of complex **1** is depicted in Fig. S7, ESI†. Experimental and calculated geometrical parameters of the complex are presented in Table 2. It is clear from the table 2 that calculated geometrical parameters are in good agreement with the experimental value except for the bond length of Cu-O2 (difference in bond length is 0.53 Å); the reason for this deviation may be due to the crystal packing arrangement. Based on the above results we have optimized the structure of complex **2** (crystal structure is not available) with the same level of theory. The calculated geometrical parameters of the complex **2** are presented in Table 2. Experimental and calculated energy of the electronic absorption band of the complex **1** and **2** with important electronic transition are given in Table 3. For complex **1** three main peaks have been observed at 287, 337 and 350 nm and the corresponding calculated values are 360, 379 and 397 nm. The orbital's (Fig. 2) involved in this transition are β - HOMO, LUMO and α -HOMO-1 and LUMO (Table 3). Similarly, for complex **2** the

two main peaks have been observed at 285 and 329 nm and the corresponding calculated values are 276 and 377 nm. HOMO, LUMO and LUMO+3 are important orbital's (Fig. 2) which is involved in the electronic transitions of this complex (Table 3). The deviation of calculated values from the experimental values is acceptable within the framework of TDDFT theory.

5 DNA interaction studies

Absorption titration

Interaction of the two metal complexes with CT-DNA was investigated by monitoring the LMCT transition of the complexes at 350nm (**1**) and 328 nm (**2**) in the presence of increasing amount of CT-DNA. Hyperchromism in the spectral band has been observed in the case of complex **1** in the presence of DNA (Fig. 3a), which is a characteristic change for non-intercalative mode of DNA binding.^{28, 29}

Metal complexes containing Itpy ligand have been shown to bind DNA intercalatively.³⁰

However, results of spectral titration do not support intercalative binding of complex **1** to DNA. It is possible that this complex binds to DNA base coordinatively. Labiality of the fifth and sixth position, especially in solution phase, is well known in the case of copper (II) complexes.³¹ In order to check the coordinative binding ability of complex **1** to DNA bases, solution of complex **1** was interacted with guanine and its ESI mass spectrum was analysed. ESI mass spectrum of the reaction mixture clearly indicates the presence of a species with m/z 573.7 (Fig. 4) which can be attributed to $[\text{Cu}(\text{Itpy})(\text{OAC})\text{G}]^+$. Complex **1** was also interacted with guanosine. In this case the ESI mass spectrum of the reaction mixture showed presence of a species with m/z 647.2 (Fig. 5) which can be attributed to $[\text{Cu}(\text{Itpy})\text{dG}]^+$. These results clearly show that complex **1** can bind to the DNA bases coordinatively. The coordinative binding of nuclear base to complex **1** has also been confirmed by monitoring the ligand field transition of complex **1** in the presence of G and dG. The ligand field band of complex **1** is centered at 665 nm. However, in the presence of G this band has been observed at 678 nm and in the presence of dG at 670 nm (Fig. S8, ESI †). In the case of complex **2** too its base binding

ability was investigated by taking ESI MS spectrum of this complex in the presence of G. In this case no mass spectral peak assignable to $[\text{Zn}(\text{Itpy})\text{G}]^+$ or $[\text{Zn}(\text{Itpy})(\text{OAc})\text{G}]^+$ could be observed. Hence, it is clear that this complex is not involved in DNA base binding. Non covalent binding of this complex to DNA has been investigated by spectral titrations. In this case, initial addition of DNA brings about 5 hyperchromism in the MLCT spectral band of complex **2**, further addition leads to the hypochromism (Fig. 3b). This observation suggests intercalation of the complex to DNA, as has been observed with many metal complexes of Itpy ligand. The DNA binding constant obtained for complexes **1** and **2** were $3.71 \pm 0.25 \times 10^4$ and 2.31×10^4 respectively, which is less than that observed for classical intercalator.³²

10 Circular dichroism

CD spectra of CTDNA shows the characteristic positive cotton effect at 278 nm and a negative cotton effect at 249 nm, corresponding to the base stacking and the helicity of normal B-DNA conformation.³³⁻³⁵ Same concentrations of complexes **1** and **2** were incubated with the CT DNA, in order to study the conformation changes in DNA upon binding of these metal complexes. Control 15 experiment of DNA+Cu²⁺, DNA+Zn²⁺ and DNA+Itpy ligand did not show any appreciable conformational change in DNA. On the other hand both the complexes brought about significant change in the negative band of DNA (Fig. 6). In the presence of complex **1** there is a marginal decrease in the intensity of the positive band of DNA (Fig. 6a). However, in the presence of complex **2** the intensity of the positive band has been found to increase along with 3 nm red shift in the band position 20 (Fig. 6b). Usually intercalative mode of binding enhances the positive cotton effect, as has been observed in this case. Hence, results of these experiments indicate that complex **1** binds DNA non intercalatively and complex **2** binds DNA intercalatively. It is also clear that binding of the two complexes leads to change in the helicity of DNA.^{36, 37}

DNA cleavage studies

Agarose gel electrophoresis was performed using pUC19 plasmid DNA in the absence and presence of the two complexes. Control experiments such as DNA+H₂O₂, DNA+Itpy, and DNA+Zn²⁺ did not show DNA cleavage (Fig. S9, ESI†). In the presence of Cu²⁺+H₂O₂+DNA marginal DNA cleavage has been observed (Fig. S9, ESI†). In the absence of any external agent complex **1** did not bring about any DNA cleavage. In the presence of external agent H₂O₂ complex **1** brought about efficient DNA cleavage (Fig. 7a). Even at low complex **1** concentration of 0.5 μM, form III DNA was formed. Fig. 7a shows concentration dependent DNA cleaving efficiency of complex **1** in the presence of H₂O₂. With increase in the concentration of complex **1**, gradual increase in the conversion of form II DNA to form III was observed. In order to identify the species responsible for the cleavage of DNA, the experiment has been carried out in the presence of DMSO, which is a known hydroxyl ion scavenger. In the presence of DMSO no DNA cleavage has been observed indicating that hydroxyl ion is responsible for the cleavage of DNA in the presence of complex **1** and H₂O₂ (Fig. S9, ESI†). This clearly shows that hydroxyl radical produced by the complex and hydrogen peroxide is responsible for the observed DNA cleavage in the presence of these two reagents. In the case of complex **2**, even in the absence of any co-reagent DNA cleavage has been observed after 6 hr incubation time (Fig. 7b). In this case too, a metal complex concentration dependent DNA cleavage has been observed as shown in Fig. 7b. Hence, it is obvious that complex **2** is capable of bringing about DNA cleavage via hydrolytic pathway.³⁸

Protein interaction studies

20 Fluorescence quenching studies

Presence of amino acids tryptophan, tyrosine and phenylalanine results in the intrinsic fluorescence of BSA (Bovine serum albumin).³⁹⁻⁴¹ Among the three amino acids; tryptophan mainly contributes to the intrinsic fluorescence of this protein. Changes in the fluorescence intensity of BSA were monitored by exciting at 295 nm (Trpy residue) in the presence of increasing amount of complexes **1** and **2**. Both the

complexes brought about rapid quenching of BSA fluorescence (Fig. 8a, b). Complex **2** not only brought about quenching of fluorescence of BSA, but also brought about a red shift of about 12 nm in the emission maxima. No such change in the energy of the emission of BSA was observed in the presence of complex **1**. This shows that the binding site of the two complexes on the protein must be different. BSA has one metal binding domain for copper which is in domain I (27 HIS), whereas zinc has multiple binding sites in domain I & II (91, 123, 270, 272 residues). Warfarin, the known domain II, subdomain site I marker shows, similar kind of red shift in the fluorescence of BSA, as observed with complex **2**.⁴² Binding of Warfarin to BSA has been attributed to the hydrophobic interaction of warfarin with amino acid residues in the site I of domain II. Hence, we can conclude that complex **2** too most probably binds to site I of domain II of BSA. Binding of complex **1** on the other hand probably takes place at the native copper binding site of BSA, which is domain I. The Stern Volmer quenching constant for the quenching of tryptophan emission of BSA by complexes **1** and **2** were 8.24×10^2 and 5.47×10^2 respectively.

Conformational changes of BSA brought about by the metal complexes

Interaction of metal complex with BSA may affect the secondary or tertiary structure of protein. Secondary structural changes of BSA influenced by the metal complexes can be studied by using CD spectral techniques. BSA, typical α -helix protein, shows two negative bands at 208 and 222 nm in CD spectrum due to $n-\pi^*$ transition from the peptide bond of α -helix.^{43, 44} Fig. 9a, b shows increasing concentration of metal complexes influenced secondary structural changes of BSA. Secondary structures of BSA were quantified using CONTIN algorithm (Table 4).⁴⁵ It can be seen from Table 4 that native BSA has 53.9% right handed helical structure. In the presence of 4 μ M complex **1** the right handed helical content slightly increases. Further increase in the concentration of complex **1** result in decrease in the right handed helical content to 0% and increase in the distorted helical content. However, further increase in the concentration of complex **1** to 30 μ M results again in an increase in

the right handed helical content to 69%. In the presence of complex **2** however, there is a decrease in the right handed helical content even at the highest concentration of the complex used (30 μ M). In this case, the protein confirmation finally changes to distorted strand. Control experiment of free ligand+BSA does not show any conformational changes in BSA, where as in the presence of free Cu^{2+} and Zn^{2+} marginal deformation in the BSA conformation has been observed (Fig. S10, ESI†).

Molecular modelling studies

Molecular docking calculations were performed using BSA as model system. Molecular docked image of the complexes located within the hydrophobic cavity of BSA are shown in Fig. 10. In the cavity, complexes were surrounded by the hydrophobic as well as charged residues of the amino acids. The binding energy of the two complexes with BSA, nearby amino acids and the hydrogen bond distances are shown in Table S1. Three different types of hydrogen bonding have been observed between the complex **1** (COO, imidazole (NH) and pyridine (N)) and polar amino acid residues (N, -NH and O). These three hydrogen bonds are (i) between His-145(N-H)–Itpy (N) pyridine (3.5 Å), Glu-424(COO)-N of (Pyridine Itpy) (3.3 Å), (ii) Arg-458(NH₂)- Acetate COO (2.8 Å), Arg-458(NH₂)- Acetate COO (3.2 Å), Lys-431(NH)- Acetate COO (3.4 Å) and (iii) Ser-428(O of OH)-Imidazole (Itpy) (2.2 Å), Arg144(N)-Imidazole (Itpy) (2.1 Å), Ser-192(O)-Imidazole (Itpy) (2.4 Å), Ser-192(O)-N-H imidazole (Itpy) (2.3 Å). In the case of complex **2** two types of hydrogen bonding were observed (i) between the residues Arg-144(NH)- Acetate COO (3.5Å), Arg-458(NH)- Acetate COO (2.9Å), Arg-458(NH)- Acetate COO (3.4Å), Ser-428(O)-N-H (Itpy) (2.8Å), Ser-192(O)- Acetate COO (3Å), His-145(NH)- Acetate COO (3.4 Å), Arg-458(NH)- Acetate COO (3.1 Å), Arg-185(NH)- Acetate COO (3.1Å) and (ii) Ser-192(O)-N-H (Itpy) (2 Å), Arg-144(N)-N-H imidazole (Itpy)(2.6) . From these results it can be inferred that the interacting residues for the two complexes are different. Complex **1** and **2** both interact with the polar amino acids in the deep hydrophobic cavities of BSA. Hydrogen bonding and Vander Waals interaction are the main driving forces of interactions.

Cytotoxicity

Cell proliferation

Cytotoxicity of the complexes was tested against A549 lung cancer cell line using MTT assay. From the percentage cell growth inhibition vs. complex concentration plot (Fig. S11, ESI[†]), dose dependent cell death inducing ability of the complexes has been observed. The IC₅₀ values of complex **1** (8.43 μ M), is higher than that of the complex **2** (5.83 μ M), which indicates that the metal ion does play a role in the observed cytotoxicity of the two metal complexes. It is noteworthy that complex **1** which had greater DNA binding constant K_b value compared to complex **2**, showed lower cytotoxicity among the two complexes. Such behaviour has been reported by Barone et al., recently.⁴⁶ Lower IC₅₀ value for Zn(II) complex compared to the Cu(II) complex of the same ligand has also been reported for complexes of diethyl-2,2'-(((3-(((5H-indolo[3,2-c]quinolin-6(1H)-ylidene)-hydrazono)methyl)-2-hydroxy-5-methylbenzyl)azanediyl)-diacetate⁴⁷.

Dual Staining assay

To assess the type of cell death induced by the complex **1** and **2** in A549 cells, the morphological changes after double staining with Acridine Orange/Ethidium Bromide (AO/EB) were investigated (Fig. 11 & 12). AO/EB staining uses combination of two dyes to visualize cells with aberrant chromatin organization.⁴⁸ AO penetrates into living cells, emitting green fluorescence after intercalation into DNA, but it cannot distinguish viable from non-viable cells. EB on the other hand is able to permeate the altered cell membrane of dead cells and emit red fluorescence. A mixture of 20 Acridine Orange and Ethidium Bromide was used to distinguish between live and dead cells. The differential uptake of these two dyes allows the identification of viable and non-viable cells. Normal cells showed uniformly green-fluorescing nuclei with a highly organized structure. On the other hand complex **1** and **2** treated cells exhibited green as well as red fluorescence indicating that both these complexes brought about cell damage due to loss of cell membrane integrity. Since initial stages of

apoptosis results in loss of membrane integrity our observations indicate that the cells are undergoing apoptosis. From Fig. 11 one can see that as the concentration of complex **1** increase from 6 μM to 10 μM the intensity of green fluorescence due to AO stain decreases, indicating that population of live cells decrease with increase in the concentration of complex **1**. In the presence of 8 μM complex **1** 5 bright green patches are seen, which is an indication of early apoptosis ⁴⁹. It can also be seen from Fig. 11 that as the complex concentration increases, the orange fluorescence due to EB stain increases, indicating an increase in the population of dead cells. Fluorescence microscopy images of cells treated with complex **2** shown in Fig. 12 clearly indicate that in this case even 3.9 μM of the complex is able to bring about early apoptosis, as evident from the bright green patches in the AO stained image and 10 orange red in EB stained image.

Propidium Iodide – nuclear fragmentation assay

Apoptosis was further confirmed by analyzing the nuclear morphology of A549 cells which had been treated with complexes **1** and **2**. Nuclear morphology was evaluated with membrane-permeable PI stain ⁵⁰ and the results are shown in Fig. 11 and 12. The morphology of complex **1** treated cells, 15 particularly at 10 μM , clearly displays characteristic features of reduced size, intense fluorescence of condensed nuclear chromatin and formation of membrane blebs, which are typical of late apoptosis or necrosis ⁵¹. On the other hand normal cells are of uniform morphology without any nuclear condensation. Results of PI staining of complex **2** treated cells show initial nuclear condensation, blebbing and apoptotic body formation at 7.8 μM of the complex, which is typical of late apoptosis or 20 necrosis. The effects of concentration of the two complexes on their ability to induce apoptosis to A549 cells are shown in Fig. S12, ESI†. It is clear from the Fig. S12, ESI† that as the concentration of the metal complex increases the percentage of cells undergoing apoptosis also increases. There are many mechanisms by which cells undergo apoptosis. No attempt has been made in this study to understand the mechanism of apoptosis brought about by the two metal complexes.

Conclusions

Two metal complexes, [Cu(itpy)(OAc)(H₂O)] NO₃ (**1**) and [Zn(itpy)(OAc)]OAc (**2**) which have the same ligand environment but different central metal ions, have been synthesised to understand the role of metal ion in the DNA/Protein binding, DNA cleaving ability and the cytotoxicity of the complexes. These two complexes have been characterised using electronic spectroscopy and ESI mass spectroscopy. The complex **1** has also been characterised crystallographically. The copper(II) complex **1** has been found to bind to nuclear bases and nucleosides coordinatively, indicating that they have the ability to bind to DNA bases coordinatively. The zinc(II) complex **2** on the other hand, has been found to bind to DNA intercalatively. Complex **1**, due to the redox active nature of the central copper (II) ion, brings about oxidative cleavage of plasmid DNA. Complex **2** which has the redox inactive central metal ion Zn (II), did not promote any oxidative cleavage of DNA. This complex however, is able to bring about hydrolytic cleavage of DNA. Complexes **1** and **2** have been found to bind to BSA. However, they bind to different domains in the protein. Both these complexes have been found to be cytotoxic towards A549 lung cancerous cell line. The Zinc(II) complex has been found to be more cytotoxic than the copper(II) complex; the IC₅₀ values of the two complexes being 5.83 μM for complex **2** and 8.43 μM complex **1**. Both these complexes have been found to bring about apoptosis of the A549 cells.

Experimental methods

Materials

The materials used in this investigation such as 2-acetyl pyridine, imidazole-2-carboxaldehyde, copper acetate and zinc acetate were purchased from Aldrich Chemicals and used as received. CT DNA and BSA were purchased from Sigma Aldrich. Other materials like sodium hydroxide, ammonium acetate and solvents like methanol, acetonitrile were of reagent grade. The ligands 4'-(imidazole)-2,2':6,2'-

terpyridine was prepared by minor modification of previously reported procedure for the synthesis of phenyl terpyridine (ESI†).⁵² A stock solution of CT DNA in 10 mM, Tris buffer (pH = 7.2) gave a ratio of UV absorbance 1.8–1.9 at A260/A280 nm, indicating that the DNA was sufficiently free of protein and the concentration of DNA was determined by measuring the absorbance at 260 nm. Stock solutions were stored at 4° C and used within 4 days. Plasmid pUC19 DNA was purchased from Bangalore Genei, India. Milli-Q water was used to prepare the solutions. Human lung adenocarcinoma A549 was purchased from National Centre for Cell Science, Pune, India. A549 cell line was grown in DMEM (Dulbecco's Modified Eagle's Medium), containing 2 mM glutamine, 0.55 mM L-arginine, 0.24 mM L-asparagine monohydrate supplemented with 10% heat inactivated Fetal Calf Serum (FCS) and antibiotics penicillin/streptomycin/gentamicin. All materials were of analytical grade and used without further purification unless otherwise noted.

Methods and instrumentation

The elemental analysis was performed using a EURO EA 3000–Single CHNS analyzer. The molecular mass of the complex was recorded in an electrospray ionization (ESI) mass spectrometer. ESI mass spectra of the complexes were recorded with a Thermofinnigan LCQ-6000 Advantage Max ion trap mass spectrometer equipped with an electron spray source. Stock solutions were prepared using buffer and small amount of DMSO. In order to check for the formation of copper(II) complex-nuclear base adduct 1:2 ratio of complex **1** and G or dG have been taken in DMSO solvent and incubated for two hours before mass spectral analysis. Acetonitrile was used as a carrier solvent. The electronic spectrum of DMSO solution of the complexes was taken in a Perkin–Elmer Lambda 35 double beam spectrophotometer. The IR spectrum of the complexes was recorded using an ABB BOMEM MB 3000 FT-IR spectrophotometer and the samples were prepared by using KBr mull sampling technique. NMR spectrum of the zinc(II) complex was run on a Bruker 300 MHz NMR Spectrometer. Tetramethylsilane (TMS) was used as reference for the assignment of ¹H and ¹³C chemical shifts. The

e.p.r spectrum was recorded on a Bruker EMX 10/2.7 X-band EPR spectrometer operating at the X-band and using 100 kHz magnetic field modulation. EPR spectrum of complex **1** was run in DMSO solvent. Low temperature measurements were made using a liquid nitrogen Dewar. Electrochemical measurements were done using CH electrochemical analyzer with three electrode system. A glassy carbon working electrode, a platinum-wire auxiliary electrode, and a saturated calomel electrode (SCE) as reference electrode were used. Glassy carbon electrode surfaces were polished with alumina, sonicated in double distilled water, and air-dried immediately before use. The DMSO solution of the complexes (0.1-1.5 mM) containing 0.1 M TBAP as supporting electrolyte were placed in a single-compartment electrochemical cell and degassed by bubbling with nitrogen gas. Fluorescence of cells 10 was measured using inverted fluorescent microscope from Nikon, Japan.

Synthesis

[Cu (Itpy) (OAc) (H₂O)] (NO₃).2H₂O (**1**)

The complex was prepared by dissolving copper (II) acetate (1 mM, 182 mg) and Itpy (1 mM, 300 mg) in methanol (10 ml); the mixture was stirred for about 4 h at room temperature. Solution so obtained 15 was turbid. To this turbid solution few drops of nitric acid was added to get a clear green solution. This solution was then heated to boil. Subsequently it was cooled to get dark green compound. It was recrystallized from methanol-ether solution. Diffraction quality crystals were obtained by ether diffusion method from a methanolic solution of the complex.

Yield 82 %; Anal.Calc.For C₂₀H₂₂CuN₆O₈ ; calculated (%) C, 44.65; H, 4.12; N, 15.62. found (%): C, 20 44.48; H, 3.91; N, 15.76. FT-IR (KBr pellet) : 3385 cm⁻¹ (br., ν H₂O), The uncoordinated nitrate ion shows the band at 1380 cm⁻¹(very strong ν (NO₃)), 1480 cm⁻¹ (ν COO⁻), Peaks revealing the presence of Itpy in the complex is seen in the ranges 1621 to 1463 cm⁻¹ and 1470 to 1024 cm⁻¹ due to the ν C=N and ν C=C stretch and ν C=N and ν C=C vibrations respectively. The peaks between 795-722 cm⁻¹ shows the aromatic C-H deformation.

[Zn(Itpy)(OAc)] (OAc) (2)

Complex **2** was synthesised using similar procedure as adapted for complex **1** taking zinc (II) acetate instead of copper (II) acetate. Zinc (II) acetate (1 mM, 220 mg) and Itpy (1 mM, 300 mg) were taken in 5 methanol (10 ml); the mixture was stirred for about 4 h at room temperature. This solution was heated to boil and then solution filtered. The solid obtained after cooling was filtered and recrystallized from methanol-ether.

Yield 85%, Anal. Calcd for $\text{ZnC}_{22}\text{H}_{19}\text{O}_4\text{N}_5$: calculated (%) C, 54.73; H, 3.97; N, 14.50. found (%): C, 54.69; H, 3.87; N, 14.36. ^1H NMR (DMSO – d₆) δ 13.245 (s, 1H); δ 9.032 (s, 2H); δ 8.790 (d, 2H); δ 8.682 (d, 2H); δ 8.055 (t, 2H); δ 7.553 (t, 2H); δ 7.417 (s, 1H); δ 7.223 (s, 1H) (s, singlet; d, doublet; t, triplet). ^{13}C 154.012, 153.356, 147.644, 141.877, 138.159, 135.813, 122.906, 119.233, 116.409, 114.170. FT-IR (KBr pellet): 3417 cm^{-1} (br., ν H_2O), 1418 cm^{-1} & 1558 cm^{-1} (ν COO^-), Peaks revealing the presence of Itpy in the complex is seen in the ranges 1737 cm^{-1} and 1016 cm^{-1} due to the $\nu_{\text{C}=\text{N}}$ stretch and $\nu_{\text{C}=\text{C}}$ vibrations respectively. The peaks between 788-680 cm^{-1} shows the aromatic C-H deformation.

X-ray Crystallographic Data Collection and Refinement of the Structures (CCDC 787339)

A green single crystal of complex **1** of dimensions 0.05x0.04x0.03 mm^3 was coated with perfluoropolyether and immediately mounted in the nitrogen cold stream (100 K) of a Bruker APEXII diffractometer equipped with a Mo-target rotating-anode X-ray source and INCOATEC Helios mirror optics (Mo- $\text{K}\alpha$, $\lambda=0.71073\text{\AA}$). Final cell constants were obtained from a least squares fit of all integrated reflections. Crystallographic data of the compound are listed in Table 1. The Siemens ShelXTL⁵³ software package was used for solution and artwork of the structure, ShelXL97⁵⁴ was used for the refinement. The structure was readily solved by Patterson method and subsequent difference Fourier techniques. All non-hydrogen atoms were anisotropically refined. Hydrogen atoms attached to

carbon atoms were placed at calculated positions and refined as riding atoms with isotropic displacement parameters. Hydrogen atoms of coordinated and uncoordinated water molecules and the hydrogen atom bound to N (20) were localized from the difference map and were refined with restrained bond distances and displacement parameters.

5 Computational methods

DFT

The ground-state geometries of complex **1** and **2** were optimized using density functional theory (DFT) with Becke 3-parameter-Lee-Yang-Parr (B3LYP) ⁵⁵ hybrid functional and 6-31G (d) basis set. The vertical excitation energies were calculated within the framework of TD-DFT ⁵⁶ using ground-state 10 optimized geometries with the above mentioned basis set. Frequency calculations have been performed to confirm the minima on the potential energy surfaces. All calculations have been performed using Gaussian 09 package. ⁵⁷

Docking studies

15 For docking studies the structural coordinates of BSA were obtained from the protein data bank (pdb id : 4F5S). The geometries of complexes **1** and **2** were optimized with 6-31g* basis set by using b3lyp functional in Gaussian 09 package.⁵⁸ The DFT optimized geometries of ligand molecules were used in docking. Docking calculations for the two complexes were carried out using Auto Dock Vina software. Binding sites of ligand molecule was automatically detected by docking. The obtained data from 20 docking was examined by PYMOL software.⁵⁹

DNA interaction studies

Absorption spectral studies

Absorption titrations were performed by fixing the complex concentration constant (20 μ M) and varying the CTDNA concentration (0-260 μ M). To nullify the absorbance changes due to DNA, an

equal volume of DNA was added to both the reference cell and the sample cells. Titration was extended till the saturation point. From the absorption titration studies, the intrinsic binding constant K_b was determined using the following equation,

$$[DNA]/(\epsilon_a - \epsilon_f) = [DNA]/(\epsilon_b - \epsilon_f) + 1/K_b(\epsilon_b - \epsilon_f)$$

Where, ϵ_a , ϵ_f and ϵ_b correspond to the apparent extinction coefficient of the complex, $A_{obs}/[\text{complex}]$, the extinction coefficient for the free complexes, and the extinction coefficient for the complex in the fully bound form. A plot of $[DNA]/(\epsilon_a - \epsilon_f)$ versus $[DNA]$ was drawn and the ratio of slope to intercept was calculated which gave K_b , the intrinsic binding constant.

Circular dichroism

CD spectra of CT DNA and BSA were analysed in the presence of increasing concentration of the two metal complexes using JASCO J-815 CD spectrometer with 150W Xe arc lamp. The instrument was controlled by Jasco's Spectra Manage software. Quartz cells having path length of 0.1 cm were used and a scanning speed of 200 nm min⁻¹ was selected. The data were expressed in terms of mean residue ellipticity (MRE). Appropriate buffer solution running under the same conditions was taken as blank and subtracted from the sample spectra. All CD spectra were taken as the average of three independent scans. Spectra were run between 235 to 330 nm for DNA in the presence of the two complexes at $r = 0.25$ and 0.5 ($r = [\text{complex}]/[\text{DNA}]$). The CD measurements of BSA (20 μM) in the absence and presence of complexes (4, 10, 15 and 20 μM) were recorded in the range of 260–200 nm.

Fluorescence quenching titration

BSA has tryptophan and binding of any small molecule to BSA can be investigated by monitoring the tryptophan emission as a function of concentration of the small molecule. In this case, the emission of BSA (20 μM) due to tryptophan at 350 nm was measured as a function of concentration of complexes

1 (0-20 μM) and **2** (0-30 μM). The quenching constant were calculated from the Stern–Volmer equation.

$$I_0/I = 1 + K_{sv} [\text{complex}]$$

Where I_0 and I represent the fluorescence intensities in the absence and presence of quencher, respectively. K_{sv} is the linear Stern–Volmer quenching constant.

Antiproliferative activity

Cell culture.

The human cancer cell line A549 was purchased from NCCS Pune. The A549 cells were grown in a RPMI 1640 medium supplemented with 10% fetal bovine serum and antibiotics. For the MTT assay, 10 cells were grown in 25 cm \times 25 cm \times 25 cm tissue culture flasks containing RPMI1640 medium as culture medium supplemented with 10% FCS, 100 U/ml penicillin, 100 $\mu\text{g/ml}$ streptomycin (GIBCO) and grown at 37°C under a humidified atmosphere of 95% air and 5% CO_2 . Cells were allowed to adhere for 4 h and when cell density in the culture flask reached 70-80% confluence, they were trypsinized and seeded in 96-well plates. Each well had a cell density of 3×10^4 cells and they were 15 grown for 24 h.

Cytotoxicity assay.

MTT assay was performed following the method described by Carmichael *et al.*,⁶⁰ and percentage of cell viability was determined by spectrophotometric determination of accumulated formazan derivative 20 in treated cells at 570 nm in comparison with the untreated ones. Test complexes **1** (0-200 μM) and **2** (0-500 μM) were added as 2X concentration to the cell in 100 μl volume. Since the compounds are soluble in DMSO, appropriate amounts of compounds were weighed and dissolved in DMSO and further dilutions were in the media. The plates were further incubated for 48 hours in the CO_2 incubator. MTT solution was composed of 3-(4,5-dimethylthiazol-2-yl)-2,5-diphenyl tetrazolium

bromide (MTT) at 5 mg/ml in phosphate buffered saline (1.5 mM KH₂PO₄, 6.5 mM Na₂HPO₄, 137 mM NaCl, 2.7 mM KCl; pH 7.4). From this solution 50 µl was pipette out into each well to achieve 1 mg/ml as final concentration. The plate was further incubated for 2.30 hours in incubator and the medium was carefully decanted. The formazan crystals were air dried in dark place and dissolved in 5 100 µl DMSO and the plates were mildly shaken at room temperature and the OD was measured using Synergy H4 micro plate reader at 570 nm. From the optical densities the percentage growths were calculated using the following formula

$$\text{Percentage growth} = \frac{100 \times (T - T_o)}{(C - T_o)}$$

Where T is optical density of test; C is the optical density of control; T₀ is the optical density at time zero.

10

Cellular morphology assessment. Acridine orange/Ethidium bromide (AO/EB) (Dual staining).

Ethidium bromide/acridine orange staining was carried out by the method of Gohelet al.,⁶¹ A549 cells were plated at a density of 5×10⁴ in 6-well plates. They were allowed to grow at 37°C in a humidified CO₂ incubator until they were 70–80% confluent. Then cells were treated with different concentrations 15 of complex **1** (6, 8 and 10 µM) and **2** (3.91, 7.81 and 15.63 µM) for 24 h. The culture medium was aspirated from each well and cells were gently rinsed twice with PBS at room temperature. Then equal volumes of cells from control and metal complex treated were mixed with 100 µl of dye mixture (1:1) of ethidium bromide and acridine orange and viewed immediately by fluorescence microscopy. The percentage of apoptotic cells was determined by the equation, % of apoptotic cells = (total number of 20 apoptotic cells/total number of cells counted) ×100.

Propidium iodide staining (PI).

Propidium iodide staining was carried out by the method of Chandramohan et al⁶². A549 cells were

plated at a density of 5×10^4 in 6-well plates. They were allowed to grow at 37°C in a humidified CO₂ incubator until they were 70–80% confluent. Then cells were treated with different concentrations of complex **1** (6, 8 and 10 µM) and **2** (3.91, 7.81 and 15.63 µM) for 24 h. Culture medium was aspirated from each well and cells were gently rinsed twice with PBS at room temperature, before fixing in 5 methanol: acetic acid (3:1 v/v) for 10 min, and stained with 50 µg/ml propidium iodide for 20 min. Nuclear morphology of apoptotic cells with condensed/fragmented nuclei was examined by fluorescence microscopy and at least 1×10^3 cells were counted for assessing apoptotic cell death.

Acknowledgment

10 One of the authors VMM thanks CSIR-India for Senior Research Fellowship. The research support from CSIR XII Plan project STRAIT is acknowledged. CLRI Communication Number: 1059.

Notes and references

^a Chemical Laboratory, Central Leather Research Institute, Council of Scientific and Industrial
15 Research, Adyar, Chennai 600 020, India. Fax: +91 44 24911589; Tel: +91 44 24411630; E-mail:
bunair@clri.res.in, bunninair@gmail.com

^b Max-Planck Institut Für Bioanorganische Chemie, D-45470 Mülheim an der Ruhr, Germany.

^c Herbal and Indian Medicine Research Laboratory, Department of Biochemistry, Sri Ramachandra University, Porur, Chennai 600116, India.

20

1 Y. Kidani, *Gan To Kagaku ryoho*, 1983, **10**, 2442.

2 B. rosenberg, *Naturwissenschaften*, 1973, **60**, 399.

- 3 R. J. Speer, H. Ridgway, L. M. Hall, D. P. Stewart, K. E. Howe, D. Z. Lieberman, A. D. Newman and J. M. Hill, *Cancer Chemother Rep*, 1975, **59**, 629.
- 4 B. Drewinko and L. Y. Yang, *Chem Biol Interact*, 1986, **60**, 159.
- 5 P. C. Hydes and M. J. Russell, *Cancer Metastasis Rev*, 1988, **7**, 67.
- 5 6. X. Sun, C. N. Tsang and H. Sun, *Metallomics*, 2009, **1**, 25.
- 7 Q. He, C. H. Liang and S. J. Lippard, *Proc. Natl. Acad. Sci. U. S. A.*, 2000, **97**, 5768.
- 8 D. B. Zamble, Y. Mikata, C. H. Eng, K. E. Sandman and S. J. Lippard, *J. Inorg. Biochem*, 2002, **91**, 451.
- 9 A. W. Prestayko, J. C. D'Aoust, B. F. Issell, and S. T. Crooke, () *Cancer Treat. Rev.*, 1979, **6**, 17.
- 10 10 M. Galanski, M. A. Jakupiec and B. K. Keppler, *Curr. Med. Chem.* 2005, **12**, 2075.
- 11 D. Wang, S. Lippard, *J. Nat. Rev. Drug Discovery*, 2005, **4**, 307.
- 12 E. L. Hegg and J. N. Burstyn, *Coord. Chem. Rev.* 1998, **173**, 133.
- 13 D. Magda, P. Lecane and Z. Wang, W. Hu, P. Thiemann, X. Ma, P. K. Dranchak, X. Wang, V. Lynch, W. Wei; V. Csokai, J. G. Hacia and J. L. Sessler, *Cancer Res.*, 2008, **68**, 5318.
- 15 14 E. L. M. Wong, G. S. Fang, C. M. Che and N. Zhu, *Chem. Commun.* 2005, **36**, 4578.
- 15 A. Terenzi, M. Fanelli, G. Ambrosi, S. Amatori, V. Fusi, L. Giorgi, V. T. Liveria and G. Barone, *Dalton Trans.*, 2012, **41**, 4389.
- 16 J. Osredkar and N. Sustar, *J. Clinic Toxicol*, 2011, **S:3**,1. doi:10.4172/2161-0495.S3-001.
- 17 E. D. Harris, *Nutr Rev* 2001, **59**, 281.
- 20 18 S. J. Lippard and J. M. Berg Principles of bioinorganic chemistry. University Science Books: Mill Valley, (1994) CA.
- 19 X. Cao, S. V. Antonyuk, S. V. Seetharaman, L. J. Whitson, A. B. Taylor, S. P. Holloway, R. W. Strange, P. A. Doucette, J. S. Valentine, A. Tiwari, L. J. Hayward, S. Padua, J. A. Cohlberg, S. S. Hasnain and P. J. Hart, *Journal of Biological Chemistry*, 2008, **283**, **23**, 16169.

- 20 L. Leinartaite, K. Saraboji, A. Nordlund, D. T. Logan and M. Oliveberg, *J Am Chem Soc* 2010, **132**, 13495.
- 21 V. M. Manikandamathavan and B. U. Nair, *Eur. J. Med. Chem.*, 2013, **68**, 244.
- 22 V. M. Manikandamathavan, V. Rajapandian, A. J. Freddy, T. Weyhermuller, V. Subramanian and
5 B.U. Nair, *Eur. J. Med. Chem.* 2012, **57**, 449; G. Sathyaraj, T. Weyhermuller and B.U. Nair, *Eur. J. Med. Chem.* 2010, **45**, 284.
- 23 V. G. Vaidyanathan and B. U. Nair, *J. Inorg. Biochem.*, 2003, **95**, 334.
- 24 R. Vijayalakshmi, M. Kanthimathi, V. Subramanian and B. U. Nair, *Biochim. Biophys. Acta.*, 2000, **1475**, 157.
- 10 25 V. Uma, M. Kanthimathi, T. Weyhermuller, B. U. Nair, *J. Inorg. Biochem.*, 2005, **99**, 2299.
- 26 C.Yan Gao, X. Qiao, Z. Y. Ma, Z. G. Wang, J. Lu, J. L. Tian, J. Y. Xub and S. P. Yan, *Dalton Trans.*, 2012, **41**, 12220.
- 27 R. D.Wood, R. Nakon and R. J. Angelici, *Inorg. Chem.* 1978, **17**, 1088.
- 28 R.V. Gessner, G. J. Quigley, A. H. J. Wang, G. A. van der Marel, J. H. van Boom, A. Rich,
15 *Biochemistry*, 1985, **24**, 237.
- 29 R. Indumathy, T. Weyhermuller and B. U. Nair, *Dalton Trans.*, 2010, **39**, 2087.
- 30 V. Uma, M. Elango and B.U. Nair, *Eur. J. Inorg. Chem.* 2007, **22**, 3484.
- 31 Cotton Wilkinson Murillo Bochmann, *Advanced Inorganic Chemistry*, Wiley India Pvt Ltd (2012)
- 32 A. E. Friedmann, J. C. Chambron, J. P. Sauvage, N. J. Turro and J. K. Barton, *J. Am. Chem. Soc.*
20 1990, **112**, 49604962.
- 33 Z. Wang, D.Liu and S. Dong, *Biophys.Chem.* 2000, **87**, 179.
- 34 Y. Zhou and Y.Li, *Biophys.Chem.* 2004, **107**, 273.
- 35 V. I. Ivanov, L. E. Minchenkova, A. K. Schyolkina and A. I. Poletayev, *Biopolymers* 1973, **12**, 89.
- 36 O. Novakova, H. Chen, O. Vrana, A. Rodger, P. J. Sadler and V. Brabec, *Biochemistry*, 2003, **42**,
25 11544–11554.

- 37 B. Norden and F. Tjerneld, *Biopolymers*, 1982, **21**, 1713–1734.
- 38 V.M. Manikandamathavan, M. Kavitha, V. Uma, R.P. Parameswari , Hannah R. Vasanthi and Balachandran Unni Nair, *Polyhedron*, 2011, **30**, 1604.
- 39 K. A. Z. Osama and I. K. A. S. H. Othman, *J. Am. Chem. Soc.* 2008, **130**, 10793.
- 5 40 G. Sudlow, D. J. Birkett and D. N. Wade, *Mol. Pharmacol.* 1976, **12** 1052.
- 41 S. Wanwimolruk, D. J. Birkett and P.M. Brooks, *Mol. Pharmacol.* 1983, **24**, 458.
- 42 Y. Z. Zhanga, B. Zhoub, X. P. Zhanga, P. Huanga, C. H. Li and Y. Liua, *Journal of Hazardous Materials*, 2009, **163**, 1345.
- 43 J. Q. Liu, J. N. Tian and X. Tian, *Bioorg. Med. Chem.* 2004, **12**, 469.
- 10 44 B. Ranjbar, and P. Gill, *Chem Biol Drug Des* 2009, **74**, 101.
- 45 N. Sreerama and R. W. Woody, *Anal. Biochem.* 2000,**287**, 243.
- 46 A. Terenzi, M. Fanelli, G. Ambrosi, S. Amatori, V. Fusi, L. Giorgi, V. T. Liveria and G. Barone, *Dalton Trans.*, 2012, **41**, 4389.
- 47 M. F. Primik, S. Göschl, S. M. Meier, N. Eberherr, M. A. Jakupec, É. A. Enyedy, G. Novitchi and
15 V. B. Arion, *Inorg. Chem.* 2013, **52**, 10137.
- 48 J. Steigerova, J. Oklestkova, M. Levkova, L. Rarova, Z. Kolar, M. Strnad, *Chem. Biol. Interact.* 2010, **188**, 487.
- 49 R. Loganathan, S. Ramakrishnan, E. Suresh, A. Riyasdeen, M.A. Akbarsha and M. Palaniandavar, *Inorg. Chem.* 2012, **51**, 5512.
- 20 50 M. J. Waring, *J. Mol. Biol.*, 1965,**13**, 269.
- 51 D. J. Arndt Jovin, and T. M. Jovin, *Methods Cell Biol* 1989, **30**, 417.
- 52 G. W. V. Cave, C. L. Raston, *J. Chem. Soc. Perkin Trans. I*, 2001, 3258.
- 53 ShelXTL V. 6.12, Bruker AXS, 2001.
- 54 G.M. Sheldrick, ShelXL97, University of Göttingen, 1997.

- 55 A.D. Becke, *Phys. Rev. A* 1988, **38**, 3098; A. D. Becke, *J. Chem. Phys.* 1993, 98, 1372; A. D. Becke, *J. Chem. Phys.* 1993, 98, 5648; C. Lee, W. Yang and R.G. Paar, *Phys. Rev. B* 1988, 37, 785.
- 56 R. E. Stratmann, G. E. Scuseria and M. J. Frisch, *J. Chem. Phys.* 1998, **109**, 8218; R. Bauernschmitt and R. Ahlrichs, *Chem. Phys. Lett.* 1996, **256**, 454.
- 57 M. J. Frisch, G. W. Trucks, H. B. Schlegel, G. E. Scuseria, M. A. Robb, J. R. Cheeseman, G. Scalmani, V. Barone, B. Mennucci, G. A. Petersson, H. Nakatsuji, M. Caricato, X. Li, H. P. Hratchian, A. F. Izmaylov, J. Bloino, G. Zheng, J. L. Sonnenberg, M. Hada, M. Ehara, K. Toyota, R. Fukuda, J. Hasegawa, M. Ishida, T. Nakajima, Y. Honda, O. Kitao, H. Nakai, T. Vreven, J. A. Montgomery, Jr., J. E. Peralta, F. Ogliaro, M. Bearpark, J. J. Heyd, E. Brothers, K. N. Kudin, V. N. Staroverov, R. Kobayashi, J. Normand, K. Raghavachari, A. Rendell, J. C. Burant, S. S. Iyengar, J. Tomasi, M. Cossi, N. Rega, J. M. Millam, M. Klene, J. E. Knox, J. B. Cross, V. Bakken, C. Adamo, J. Jaramillo, R. Gomperts, R. E. Stratmann, O. Yazyev, A. J. Austin, R. Cammi, C. Pomelli, J. W. Ochterski, R. L. Martin, K. Morokuma, V. G. Zakrzewski, G. A. Voth, P. Salvador, J. J. Dannenberg, S. Dapprich, A. D. Daniels, Ö. Farkas, J. B. Foresman, J. V. Ortiz, J. Cioslowski, and D. J. Fox, Gaussian, Inc., Wallingford CT, 2009.
- 58 W. L. DeLano, The PyMOL Molecular Graphics System, DeLano Scientific LLC, Palo Alto, CA, 2008; D. Seeliger, B.L. de Groot, *J. Comput-Aided Mol. Des.* 2010, **24**, 417; M. W. Chang, C. Ayeni, S. Breuer, B. E. Torbett, PLoS ONE 2010, **5**, 11955.
- 59 M. F. Sanner, *J. Mol. Graph. Model.* 1999, **17**, 57.
- 60 J. Carmichael, W. G. DeGraff, A. F. Gazdar, J. D. Minna and J. B. Mitchell, *Cancer Res.* 1987, **47**, 936.
- 61 A. Gohel, M. B. McCarthy, G. Gronowicz, *Endocrinology*, 1999, **140**, 5339.
- 62 K. V. P. Chandramohan, P. Gunasekaran, E. Varalakshmi, Y. Hara and S. Nagini, *Cell Biol. Int.* 2007, **31**, 599.

†Electronic Supplementary Information (ESI) available: [details of any supplementary information available should be included here]. See DOI: 10.1039/b000000x/

List of figures

Fig. 1 A) ORTEP diagram of complex **1**. B) Crystal packing arrangement of complex **1**

Fig. 2 Contour plots of HOMOs and LUMOs with the orbital energies of complex **1** and **2**

Fig. 3 Absorption spectral titration of complex **1**(A) and **2**(B) in the presence of increasing concentration of CT DNA in Tris (pH 7.2) at 25 °C. Inset: Plot of $[DNA]/(\epsilon_a - \epsilon_f)$ versus [DNA].

Fig. 4 ESI-MS spectrum of complex **1** interacted with Guanine (G) in DMSO/water mixture.

Fig. 5 ESI-MS spectrum of complex **1** interacted with Guanosine (dG) in DMSO/water mixture.

Fig. 6 CD spectrum of CT DNA (200 μ M) in the presence of complex **1** (A) and **2** (B) (50 μ M & 100 μ M) in Tris pH 7.2.

Fig. 7 A) Lane 1 DNA control; lanes 2-7 complex **1** (20, 40, 60, 80, 100, 200 μ M) + H₂O₂ (78 μ M). B) Lane 1 DNA control; lane 2-8 complex **2** (20, 40, 60, 80, 100, 200, 240 μ M).

Fig. 8 Fluorescence spectra of BSA (20 μ M) in the presence of increasing amounts of (A) complex **1** (0-30 μ M) and (B) complex **2** (0-30 μ M) in Tris buffer (pH 7.2). Inset: Plot of I_0/I vs [complex].

Fig. 9 CD spectra of BSA (20 μ M) in the presence of (A) complex **1** (4, 10, 20 and 30 μ M) and (B) in the presence of complex **2** (4, 10, 20 and 30 μ M) in Tris buffer (pH7.2).

Fig. 10 Molecular docking image of (A) complex **1** and (B) complex **2** with BSA.

Fig. 11 Fluorescence images of A549 cells treated with complexes **1** (6, 8 μ M and 10 μ M) for 24 h. Cells were co-stained with AO/EtBr (green & red) and PI (red), and the fluorescence was visualized by fluorescence microscope.

Fig. 12 Fluorescence images of A549 cells treated with complexes **2** (3.91, 7.81 μ M and 15.63 μ M) for 24 h. Cells were co-stained with AO/EtBr (green & red) and PI (red), and the fluorescence was visualized by fluorescence microscope.

List of tables

Table. 1. X-ray crystallographic parameters for complex **1**

Table.2. Important bond lengths and bond angles for complex **1**

Table. 3. Experimental and calculated electronic transition energies of complex **1** and **2**

Table. 4. CD secondary structure estimation of BSA in the presence of complex **1** and **2**

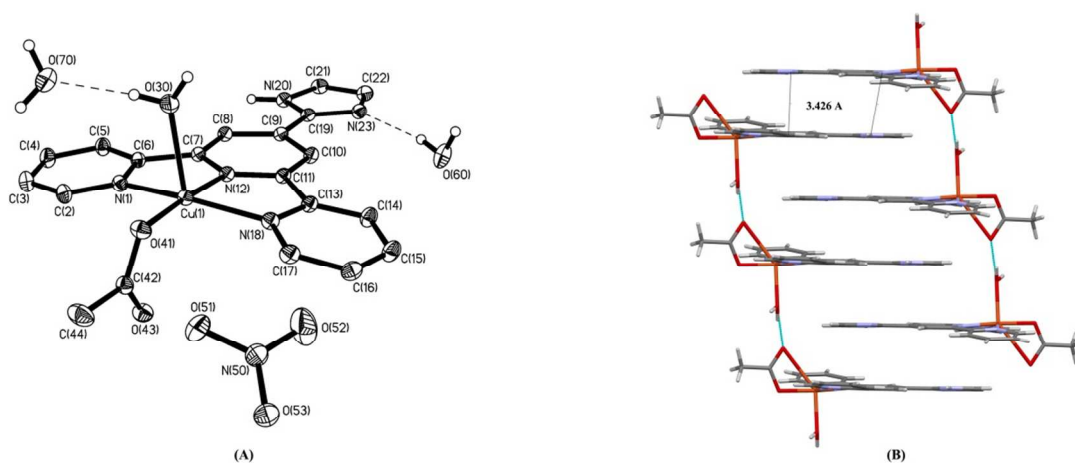


Fig. 1

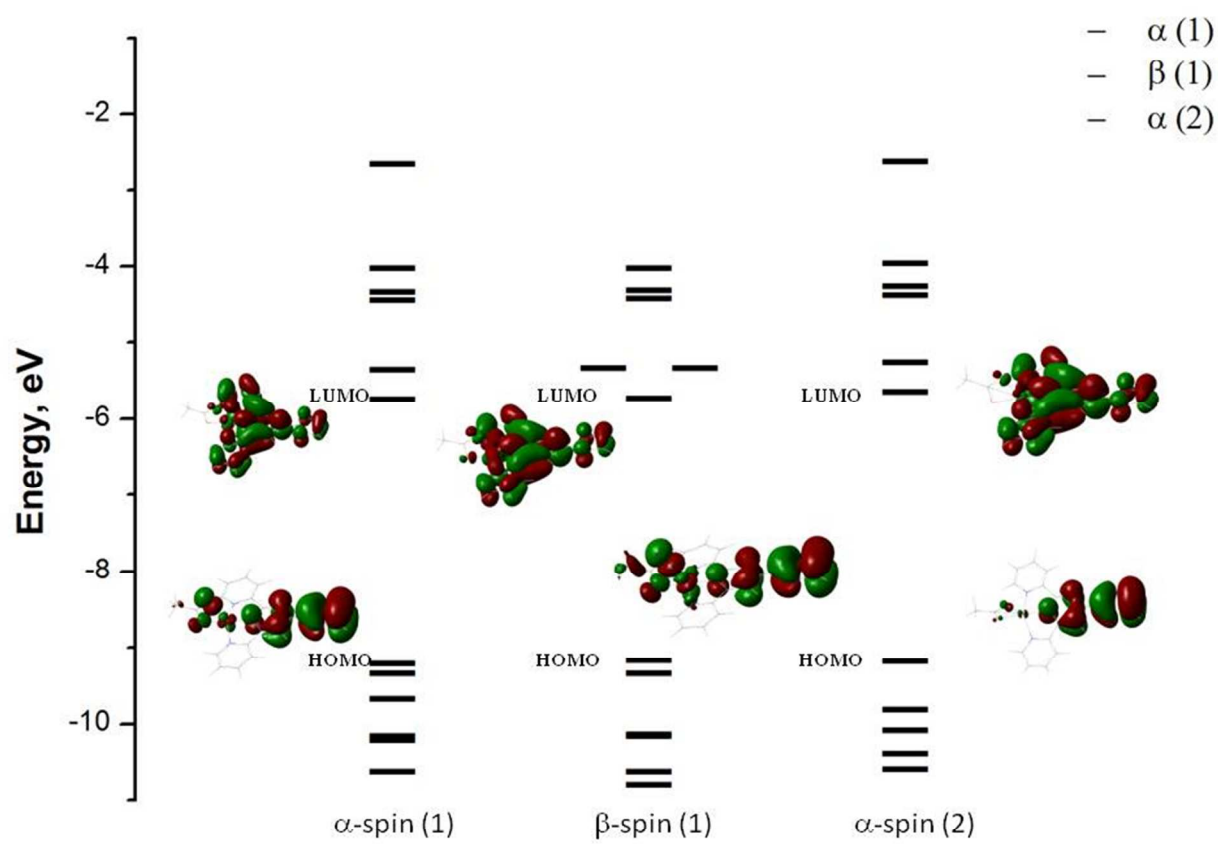


Fig. 2

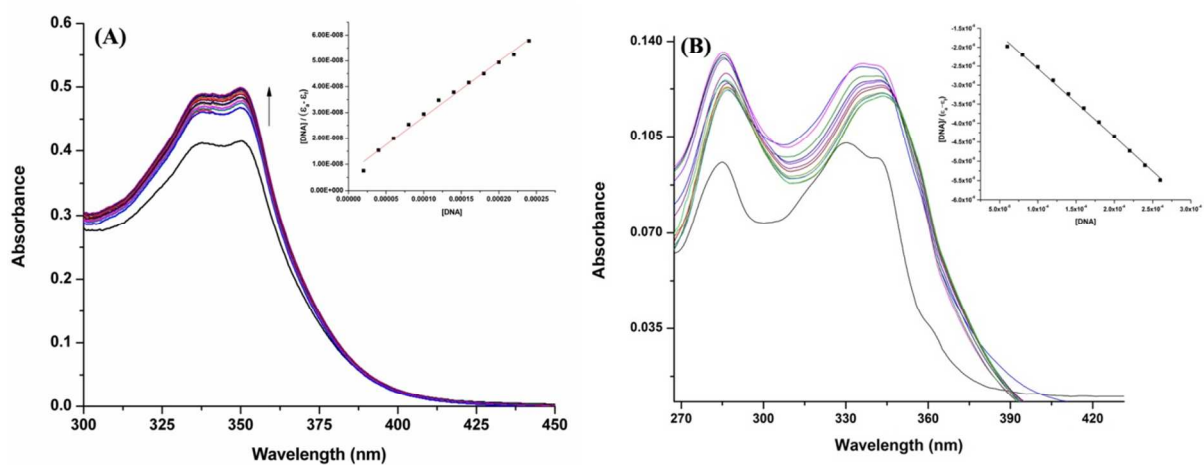


Fig. 3

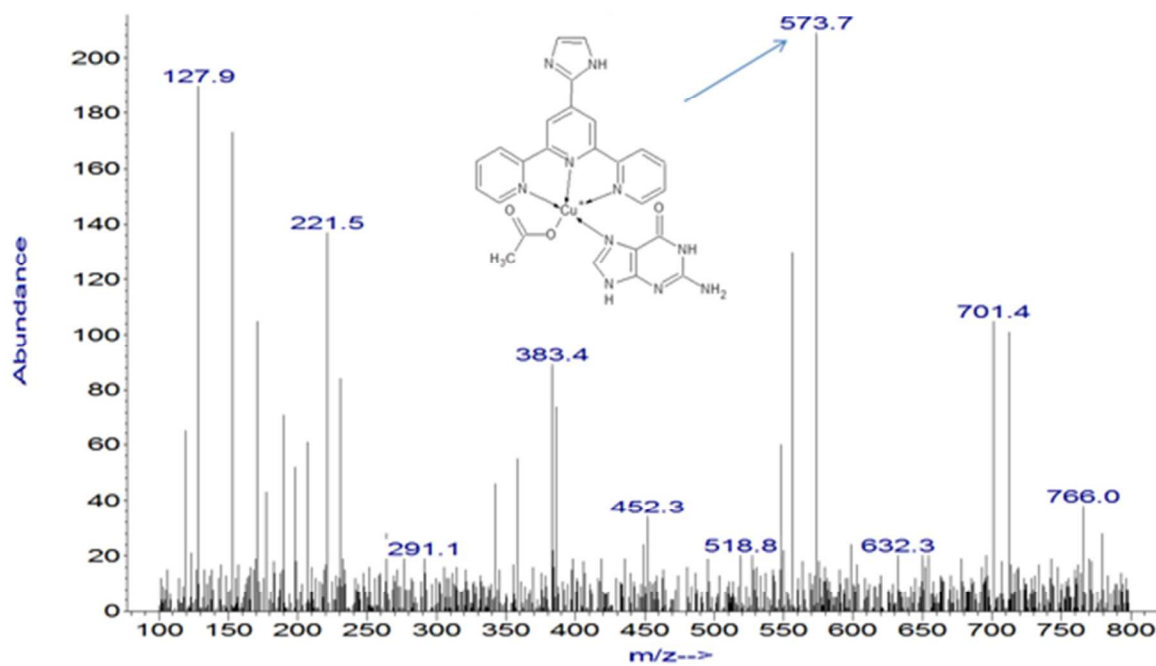


Fig. 4

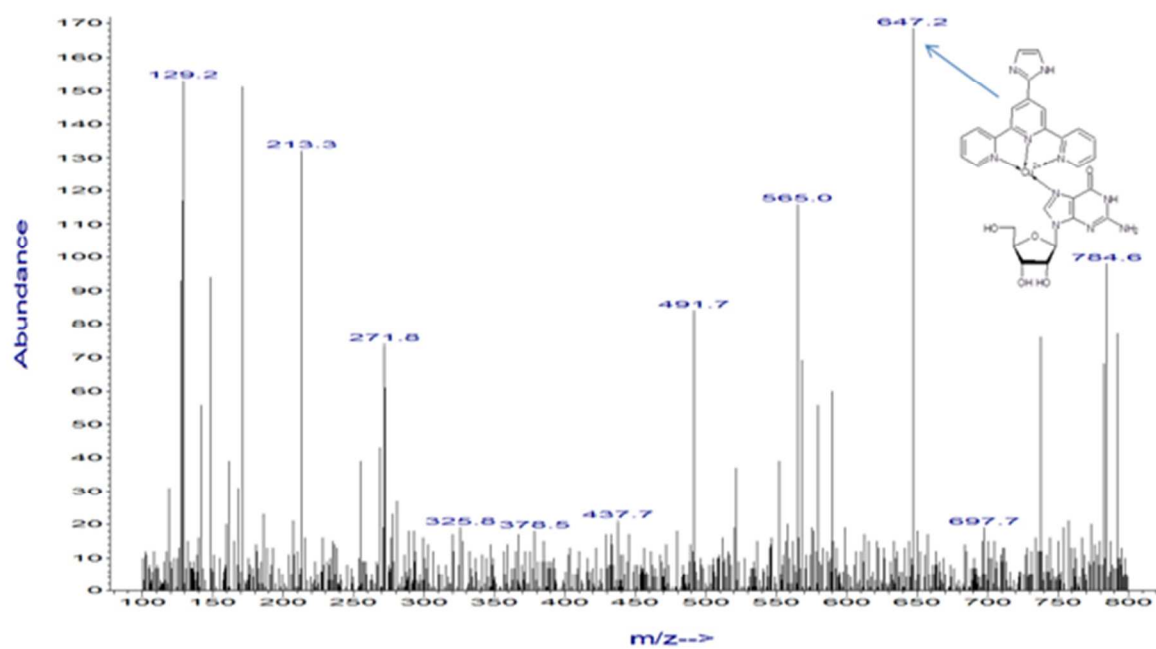


Fig. 5

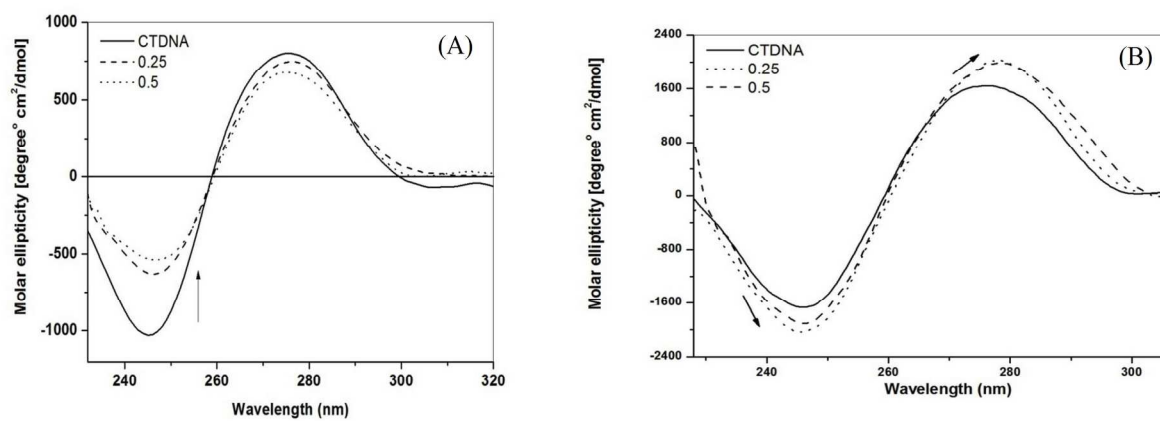


Fig. 6

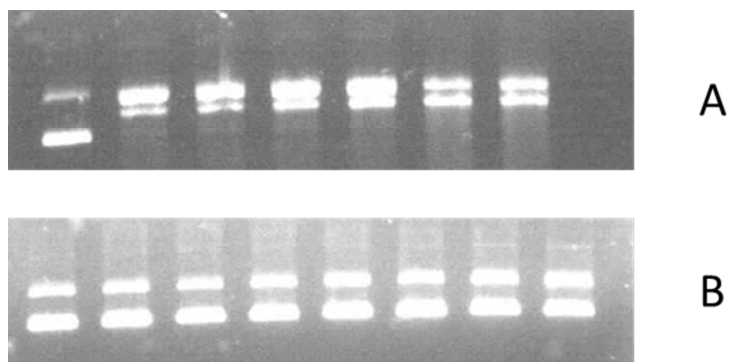


Fig. 7

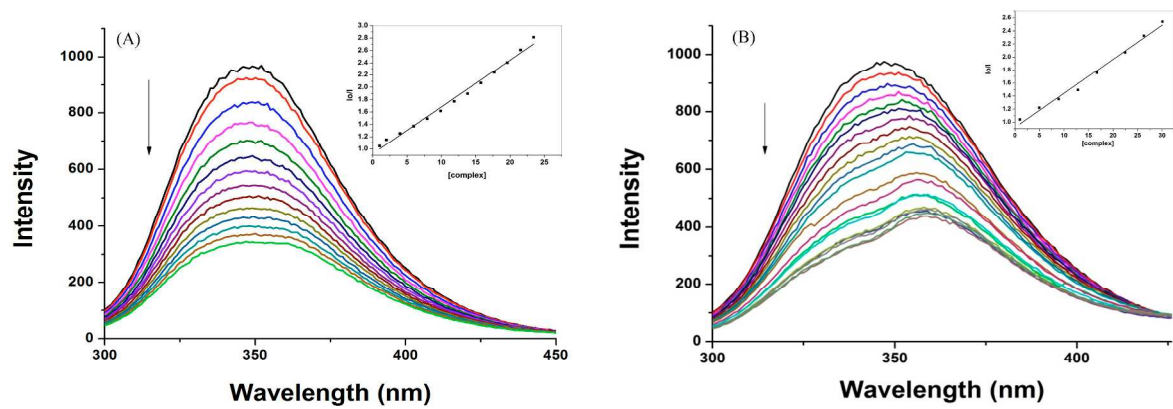


Fig. 8

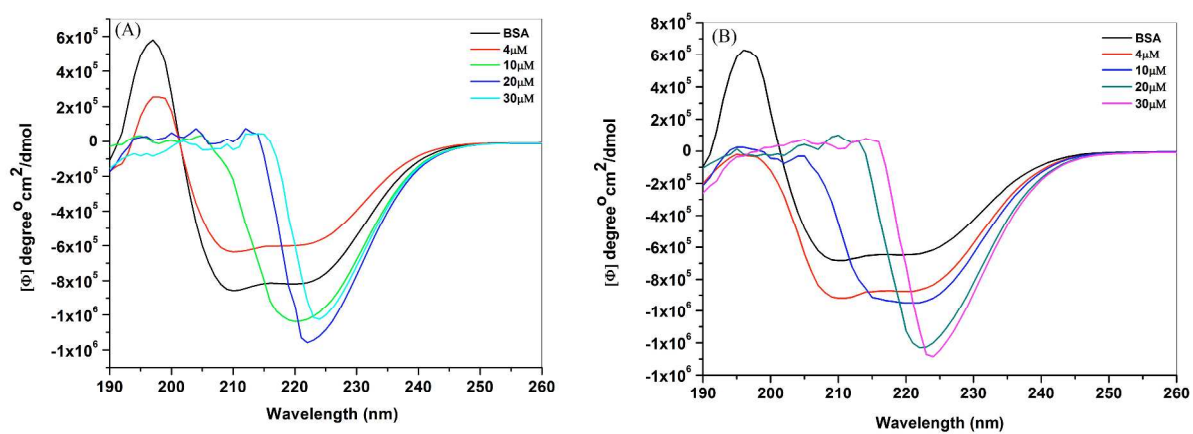


Fig. 9

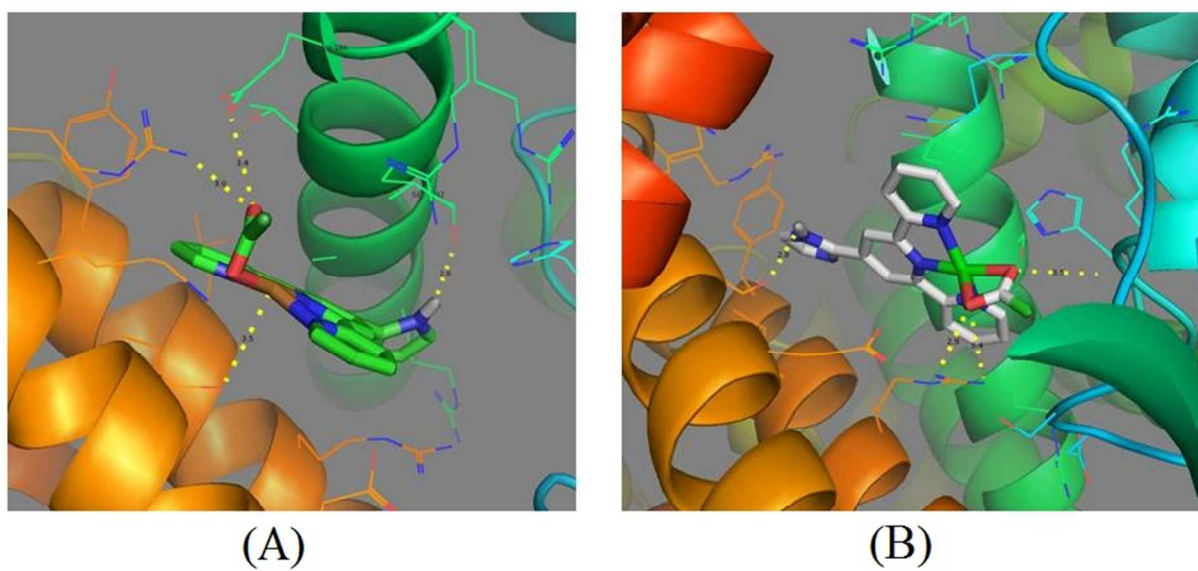


Fig. 10

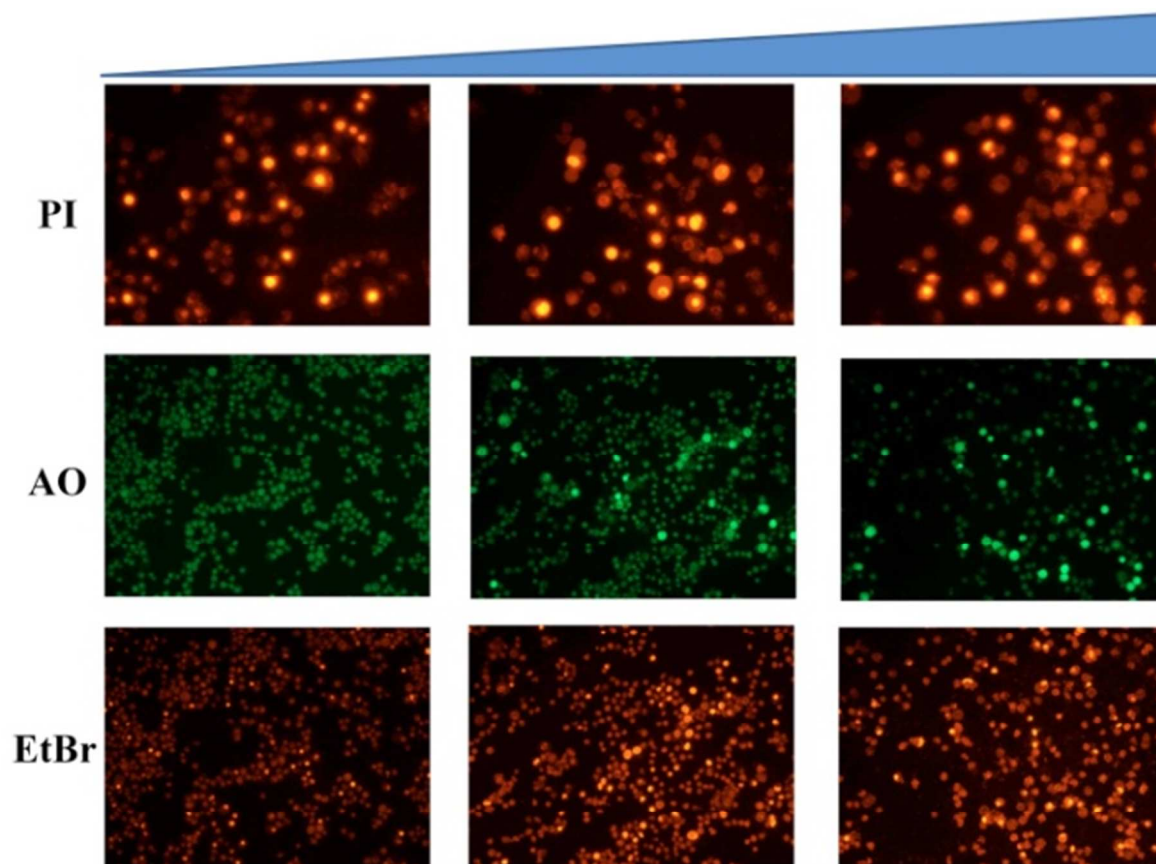


Fig. 11.

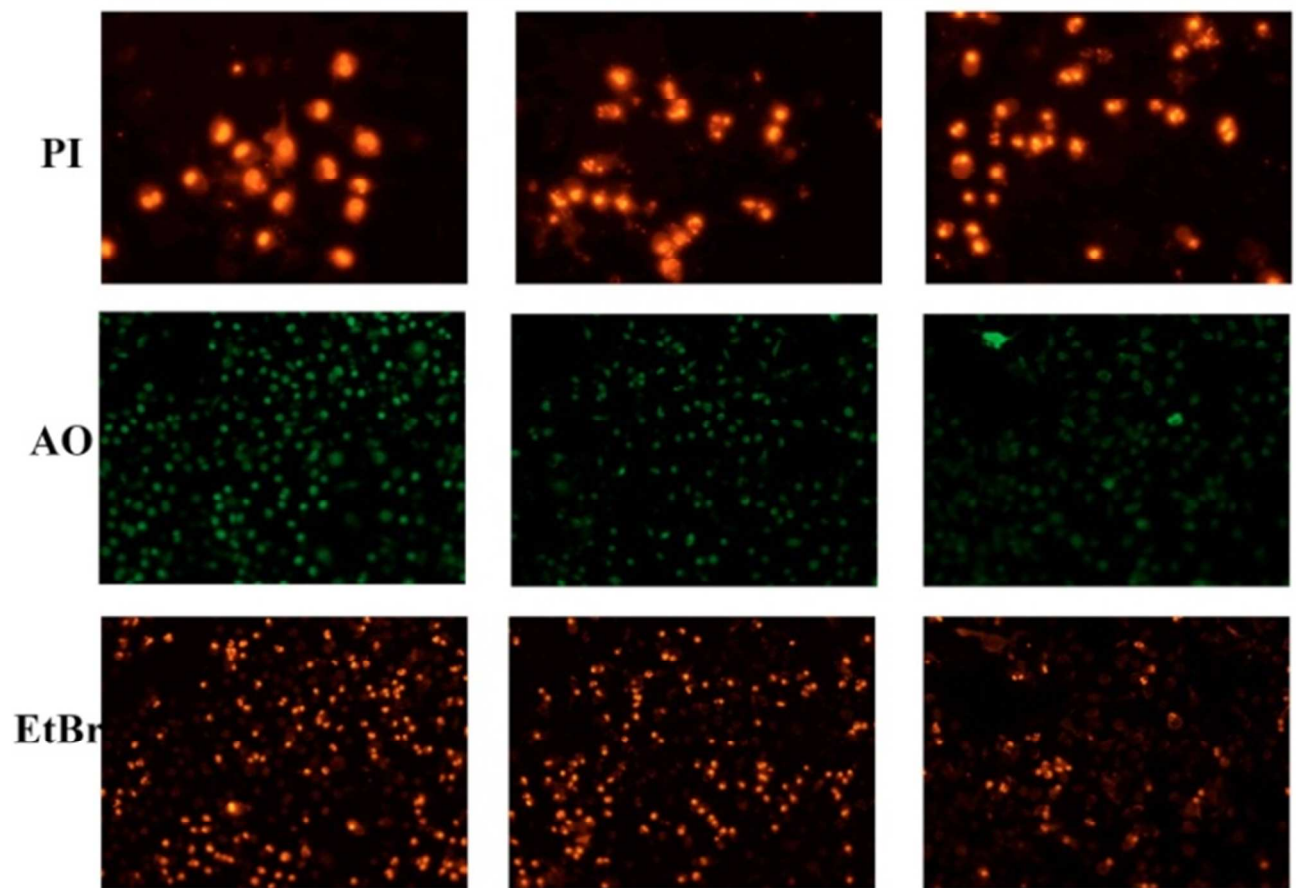


Fig. 12.

Table 1 X-ray crystallographic parameters for complex **1**

Empirical formula	C ₂₀ H ₂₂ Cu N ₆ O ₈
Formula weight	537.98
Temperature	100(2) K
Wavelength	0.71073 Å
Crystal system, space group	Monoclinic, P 2 ₁ /n, No.14
Unit cell dimensions	a = 7.0908(13) Å alpha = 90 deg. b = 22.814(4) Å beta = 102.509(3)deg. c = 14.215(3) Å gamma = 90 deg.
Volume	2244.9(7) Å ³
Z, Calculated density	4, 1.592 Mg/m ³
Absorption coefficient	1.034 mm ⁻¹
F(000)	1108
Crystal size	0.05 x 0.04 x 0.03 mm
Theta range for data collection	1.79 to 35.00 deg.
Limiting indices	-11<=h<=11, -36<=k<=36, -22<=l<=22
Reflections collected / unique	70422 / 9892 [R(int) = 0.0311]
Completeness to theta = 35.00	100.0 %
Absorption correction	Gaussian
Max. and min. Transmission	0.97261 and 0.94899
Refinement method	Full-matrix least-squares on F ²
Data / restraints / parameters	9892 / 6 / 335
Goodness-of-fit on F ²	1.039
Final R indices [I>2sigma(I)]	R1 = 0.0288, wR2 = 0.0792
R indices (all data)	R1 = 0.0335, wR2 = 0.0828
Largest diff. peak and hole	0.996 and -0.322 e.Å ⁻³

Table 2 Selected experimental (calculated) bond lengths (in Å) and angles (in °) for **1** and **2**.portant bond lengths and bond angles for complex **1** and **2**. Band gap (HOMO-LUMO) (1) 3.47 eV, (2) 3.54 eV.

Band	1		2
Cu-O1	1.920	(1.937)	(2.029)
Cu-O2	2.785	(2.255)	(2.073)
Cu-N1	2.054	(2.034)	(2.147)
Cu-N2	1.932	(1.934)	(2.045)
Cu-N3	2.045	(2.039)	(2.134)
O1-Cu-N1	100.68	(99.75)	(106.28)
O1-Cu-N2	176.00	(178.08)	(167.44)
O1-Cu-N3	99.28	(99.79)	(107.15)
O2-Cu-N1	88.99	(102.58)	(100.18)
O2-Cu-N2	123.84	(118.89)	(127.59)
O2-Cu-N3	92.61	(101.22)	(101.32)
N1-Cu-N2	79.43	(80.11)	(76.34)
N1-Cu-N3	155.86	(154.21)	(145.53)

Table 3 Experimental and calculated electronic transition energies of complex **1** and **2**

1				2			
Exp	Calc	f	Transition	Exp	Calc	f	Transition
			$\pi(\text{Itpy})/\text{O}/d_z^2 \rightarrow \pi^*(\text{Itpy})/\text{O}/d_{x-y}^2$	249	0.16	H-6	$\pi(\text{Itpy})/\text{O} \rightarrow \pi^*(\text{Itpy})$
287	280	0.06	H(β) \rightarrow L+2(β)	263	0.13	H-6 \rightarrow L+1	$\pi(\text{Itpy})/\text{O} \rightarrow \pi^*(\text{Itpy})/\text{O}/d_z^2$
337	321	0.11	H(β) \rightarrow L+1(β)	276	0.37	H-6 \rightarrow L	$\pi(\text{Itpy})/d_{xz} \rightarrow \pi^*(\text{Itpy})$
350	359	0.09	H-1(α) \rightarrow L+1(α)	317	0.17	H \rightarrow L+3	$\pi(\text{Itpy})/\rightarrow \pi^*(\text{Itpy})/\text{O}/d_z^2$
			$\pi(\text{Itpy})/d_{x-y}^2 \rightarrow \pi \rightarrow \pi^*(\text{Itpy})/d_{yz}$	366	0.09	H-2 \rightarrow L	$\pi(\text{Itpy})/d_{xz} \rightarrow \pi^*(\text{Itpy})$
				377	0.27	H \rightarrow L+1	$\pi(\text{Itpy})/d_{xz} \rightarrow \pi^*(\text{Itpy})$
						H \rightarrow L	$\pi(\text{Itpy})/d_{xz} \rightarrow \pi^*(\text{Itpy})/\text{O}/d_z^2$

^a Experimental and calculated values (in nm) of absorption energy of complex **1** and **2**

(Values in parentheses is oscillator strength of electronic transition)

Table 4 CD secondary structure estimation of BSA in the presence of complex **1** and **2**

S.No	Helix (%)		Strand (%)		Beta (%)	
	H(r)	H(d)	S(r)	S(d)	Trn	Un
(1)						
BSA	53.9	44.7	0	0	1.4	0
BSA+4 μ M	59.2	40.9	0	0	0	0
(1)						
BSA+10 μ M	0	21.6	13.9	13.0	19.1	32.4
(1)						
BSA+20 μ M	0	100	0	0	0	0
(1)						
BSA+30 μ M	69.2	28.7	1.3	0.9	0	0
(1)						
(2)						
BSA+(2)	51.4	46.2	0	0	0.024	0
BSA+4 μ M	55.7	44.3	0	0	0	0
(2)						
BSA+10 μ M	0.1	0	29.1	22.8	30.5	17.5
(2)						
BSA+20 μ M	0	0	1.7	2.3	93.7	2.3
(2)						
BSA+30 μ M	0	0	0	100	0	0
(2)						

^a H(r) – Right handed α - helix; H(d) – Distorted α –helix; S (r) – Right handed β -strand; S(d) – Distorted β -strand ; Trn – Turn; Un – Unordered

DNA/Protein interaction and cytotoxic activity of Imidazole terpyridine derived Cu(II)/Zn(II) metal complexes†

V. M. Manikandamathavan,^a T. Weyhermuller,^b R. P. Parameswari,^c M. Sathishkumar,^a
V. Subramanian,^a and Balachandran Unni Nair,^{*a}

5

Graphical Abstract

Metal centre plays an important role in the mode of DNA binding, cleavage, Protein binding and Cytotoxicity.

10

